Harmonic generation by atomic and nanoparticle precursors in a ZnS laser ablation plasma

M. Oujja, I. Lopez-Quintas, A. Benítez-Cañete, R. de Nalda, M. Castillejo*

Instituto de Química-Física "Rocasolano" (IQFR), CSIC, Serrano 119, 28006 Madrid, Spain

*marta.castillejo@iqfr.csic.es

ABSTRACT

Harmonic generation of a driving laser propagating across a laser ablation plasma serves for the diagnosis of multicomponent plumes. Here we study the contribution of atomic and nanoparticle precursors to the generation of coherent ultraviolet and vacuum ultraviolet light as low-order harmonics of the fundamental emission (1064 nm) of a Q-switched Nd:YAG laser in a nanosecond infrared ZnS laser ablation plasma. Odd harmonics from the 3rd up to the 9th order (118.2 nm) have been observed with distinct temporal and spatial characteristics which were determined by varying the delay between the ablation and driving nanosecond pulses and by spatially scanning the plasma with the focused driving beam propagating parallel to the target. At short distances from the target surface (≤ 1 mm), the harmonic intensity displays two temporal components peaked at around 250 nanoseconds and 10 microseconds. While the early component dies off quickly with increasing harmonic order and vanishes for the 9th order, the late component is notably intense for the 7th harmonic and is still clearly visible for the 9th. Spectral analysis of spontaneous plume emissions help to assign the origin of the two components. While the early plasma component is mainly

constituted by neutral Zn atoms, the late component is mostly due to nanoparticles, which upon interaction with the driving laser are subject to breakup and ionization. With the aid of calculations of the phase matching integrals within the perturbative model of optical harmonic generation, these results illustrate how atom and nanoparticle populations, with differing temporal and spatial distributions within the ablation plasma, contribute to the nonlinear medium.

1. Introduction

Harmonic generation (HG) is a well-established nonlinear optical process that yields coherent light in the short wavelength region of the spectrum [1]. Odd harmonics of a fundamental driving laser beam can be generated in centrosymmetric gaseous media, a process that is typically described by a perturbative approach when using nanosecond pulses as fundamental radiation [2]. However, with highly intense femtosecond pulses, high-order harmonics are generated [3], and in this case, the non-perturbative, three-step model adequately describes the main features of the process [4]. For fundamental radiation pulses in the nanosecond and femtosecond regimes, the quest for efficient nonlinear media enables the generation of coherent light in the vacuum ultraviolet (VUV) and extreme ultraviolet (XUV)/X-ray regions respectively, with high enough intensities to be used for fundamental studies and in practical applications [5].

Although gases have been traditionally employed in low- and high-order HG studies, latest research has revealed the advantages offered by laser ablation plasmas as nonlinear media, in terms of the increase of conversion efficiency or extension of the harmonic spectrum towards shorter wavelengths [6-9]. In fact, the presence of a variety of species in the laser plasma, from atoms to nanoparticles, offers the possibility of exploiting atomic or plasmon resonance effects to enhance the nonlinear optical response of the medium [10-14]. Particularly, as expected from the three-step model, nanoparticles can increase the efficiency of high HG in laser plasmas due to the larger cross-section of recombination of the accelerated electron with the parent particle. More generally, the characteristics of the laser ablation plasma, such as density, composition, spatial extent or degree of ionization, can be controlled through the selection of the ablation laser parameters, including wavelength, intensity, pulse duration, polarization and spatial profile of the beam, bringing the possibility to tailor its nonlinear response.

Analyses by optical emission spectroscopy (OES) and mass spectrometry have revealed that, together with atomic and molecular species, clusters and nanoparticles are common components in the nanosecond laser ablation plasmas of solid targets [15-20], and that their velocities and angular distributions are commonly dependent on their mass. In recent works we have studied low-order HG and frequency mixing in laser ablation plasmas of various types of materials using a Q-switched Nd:YAG driving laser [21-26]. Spatiotemporal control of the driving beam with respect to the position and time of the ablation event allows for the differentiation of distinct populations of species and enables the in-situ diagnosis of the complex ablation plasma environment. Further development of this method, to be used as stand alone or in combination with OES, is of interest to assist in the controlled generation of thin film and nanostructures by pulsed laser deposition (PLD). An additional element for the control of the medium and the search for HG enhancement lies in the features of the secondary plasma typically created by the driving laser, which can cause excitation, fragmentation and ionization of the precursor population.

Zinc sulfide (ZnS) is a direct II-VI wide band gap semiconductor with a broad range of applications. Thin films and nanostructures of this compound are becoming of interest for the fabrication of electrodes for solar energy conversion, nonlinear optical devices, light emitting diodes, lasers, and others [27]. PLD has been advantageously applied as a synthesis procedure for ZnS thin films and nanostructures, as it provides control routes of their crystallinity and crystal lattice (cubic or hexagonal) and morphology at nanometer scale, based on the choice of laser and deposition parameters [26-30].

Lately we have undertaken the investigation of the nanosecond laser ablation plasmas of ZnS, including its diagnosis by low-order HG, up to the 5^{th} order [22,31,32], and have related the properties of the nanostructured films grown by PLD to the composition and

dynamics of the various plume species [28]. Here, we report an investigation of the atomic and nanoparticle populations present in a ZnS ablation plasma initiated by nanosecond, infrared 1064 nm laser. The spatiotemporal distribution of the plasma species is probed through the behaviour of odd, low-order harmonics, from 3^{rd} to 9^{th} order, of a second laser of the same wavelength used as driving radiation and propagating through the plasma plume. The experimental results are compared with calculations of optical frequency up-conversion of the driving radiation in the perturbative regime in order to assess the contributions to the nonlinear medium of atom and nanoparticle populations and the effect of their differing spatial and temporal distribution within the plasma.

2. Experimental

The experimental set up (Fig. 1) is based on a system described formerly [21] and includes an ablation chamber connected to a second chamber for propagation and separation of the harmonic radiation generated by the interaction of a fundamental driving beam with the ablation plasma. ZnS ablation targets were prepared as 13 mm diameter, 2 mm thick pellets from powders supplied by Sigma Aldrich (99.99%, particle size < 10 μm) using a hydrostatic press at 8 ton/cm^2 followed by sintering at 350 ^{o}C in air for 12 h.

The targets were mounted on a rotating holder inside the ablation chamber (pressure below 10^{-5} mbar) to reduce crater formation during repetitive irradiation and were ablated at normal incidence with a Q-switched Nd:YAG laser (Spectra Physics, Quanta Ray Indi-HG, 1064 nm, pulses of 7 ns, 10 Hz) using pulse energies up to 30 mJ (fluences below 4 Jcm^{-2}). The driving laser, responsible for HG (Q-switched Nd:YAG

system, Lotis TII LS-2147, 1064 nm, pulses of 15 ns, 10 Hz), propagated across the plume perpendicularly to the ablating beam and up to 3 mm from the target surface.

The delay between the ablation event and the arrival of the driving laser pulses to the plume was electronically controlled in the 0-100 μs range with nanosecond resolution. The Gaussian driving beam was focused at the centre of the plume with a spherical lens of 20 cm focal length. The measured confocal parameter is ≈ 4 mm, and the peak intensity at focus is estimated to be in the range of 8.5×10^{10} to 4.3×10^{11} Wcm^{-2}. In addition to the temporal mapping of the ablation plume by HG, exploration of the spatial variation of its nonlinear optical response was possible by displacement of the focus along the propagation direction and along the normal to the target (*z* and *x* coordinates respectively, see Fig. 1). The generated harmonics co-propagated with the driving laser through a lithium fluoride window into the second chamber (with around the same base pressure as the ablation chamber) and were spectrally separated with a 60^{o} lithium fluoride prism which, for each harmonic, was adjusted by rotation to the appropriate incident angle of the incoming beam. Additional spectral filtering of harmonics was achieved in a 0.2 m vacuum monochromator (Acton VM-502, 1200 lines/mm grating) and the harmonic signals were measured with a sodium salicylate coated window-photomultiplier (EMI 9781B) combination attached to the exit slit.

Additionally, optical emission spectroscopy (OES) was employed to measure the spontaneous emission from the ablation plasma. It was detected at 30^{o} with respect to the *z* direction through the exit window of the ablation chamber (after removing the harmonics separation chamber shown in Fig. 1). This geometrical configuration made it possible to measure the plume OES both in the presence or absence of the driving laser. To record the spectra of the emitting plasma, the light was collected with a 20 cm focal length lens onto the entrance slit plane of a monochromator (Bentham, TMc300, 300

lines/mm grating) and measured with a time-gated intensified charge coupled device (ICCD, Andor Technologies, 2151) placed at its exit slit. Temporally resolved light collection was achieved by delaying the gate with respect to the laser ablation pulse. Plasma spectra resulted from the accumulation of over 125 laser ablation pulses.

3. Results

3.1. Characterization of 3rd to 9th harmonics in a laser ablation plasma of ZnS

HG of the fundamental driving laser was observed for the 3rd up to the 9th odd orders. The nonlinear nature of the process generating light detected in the UV-VUV range at the wavelengths of the corresponding harmonics (354.7, 212.8, 152.0 and 118.2 nm) was confirmed by measuring the dependence of the signal with the energy of the driving laser pulse. We obtained the expected power laws in the perturbative regime [22], where the intensity of the n^{th} harmonic scales with the n^{th} power of the laser intensity (see Section IV). Figure 2 displays, as an example, the case of the 5th harmonic. The slopes obtained for the range explored in the log-log plots are compatible with the value of 5 expected for the behaviour of a fifth order nonlinear process.

Each harmonic order displayed distinct temporal and spatial characteristics which were characterized by varying the temporal delay between the ablation and driving pulses and by spatially scanning the plasma plume with the focused driving beam along the *x* and *z* coordinates (Fig. 1). Fig. 3a shows the delay dependence of the normalized harmonic signals measured at a distance x= 0.6 mm from the target surface and by focusing the driving beam at the centre of the ablation plasma (z= 0). The data provide evidence of two temporal components observed for the 3rd to 7th harmonics and of only one detectable component for the 9th harmonic. For the 3rd to 7th harmonics, the early component finds its maximum value at around 250 ns, while the much broader, late

component peaks in the region of 10 μs. Only this latter component is detected for the 9^{th} harmonic. It should be noticed that early and late components of the respective harmonic orders follow the corresponding power laws, as mentioned earlier and exemplified in Fig. 2 for the 5^{th} harmonic. The relative intensity of the early to the late component is observed to decrease as the harmonic order increases from 3^{rd} to 9^{th} orders (Fig. 3a). For a laser driving peak intensity of $4x10^{11}$ Wcm^{-2}, the corresponding ratios are around 55, 1.6, 0.1 and 0.

Direct comparison of the generation efficiencies in the different harmonic orders is not straightforward, due to the broad spectral range where the harmonics are emitted. The detected signals were corrected considering the instrument spectral response that was evaluated taking into account all components of the detection system. After correction it can be claimed, within our confidence limits, that for the first temporal component the efficiencies follow a quasi-logarithmic drop with harmonic order, which is the expected behaviour in the absence of resonances. Contrarily, the late component shows an anomalous trend as a function of harmonic order, with a very low 3^{rd} harmonic emission, higher 5^{th} harmonic emission, and even higher for the 7^{th} order, to the point where the late-component emission of the 7^{th} harmonic is comparable to the 3^{rd} harmonic emission of the early component. This corresponds to a pronounced emission enhancement at 152.0 nm in the VUV region when the second temporal component of the plasma is used as nonlinear medium.

The temporal behaviour of the nonlinear response of the ablation plasma depicted in Fig. 3a merits detailed consideration. In previous works [22,25] we have attributed the multicomponent behaviour of the harmonic signal to the presence of species of different sizes in the ablation plume, ranging from neutral atoms and ions to nanoparticles moving away from the target at different velocities according to their mass. Thus, the

optimum delay for maximum harmonic signal of the two observed components is expected to increase with the distance of the driving beam to the target. We measured this dependence by collecting delay scans for the different harmonics at various distances from the target in the x= 0-3 mm range. The data corresponding to the early component of the 3^{rd} to the 7^{th} harmonic signals are shown in Fig. 3b. The linear dependence observed allowed an estimation of an average velocity of expansion of the fast nonlinear species of around 3400 m/s (represented by the continuous, straight line). Similar representation of the data for the late component of the harmonic signals (not shown) yielded a much lower average velocity of 100-200 m/s, although in this case the dispersion of the data is higher in correspondence with the larger temporal width of this delayed contribution to the harmonic signal.

The intensity of the coherent light generated at discrete wavelengths in the UV-VUV region strongly depends on the ablation pulse energy, as this controls the amount of ejected material and thus the plasma density. The behaviour is shown in Fig. 4 for the early component of the harmonic signals. A sharp increase at pulse energies above 4, 8 and 11 mJ is observed for the 3^{rd}, 5^{th} and 7^{th} harmonics respectively. Above these values the signals grow linearly with pulse energy until a certain order-dependent maximum value, where some form of saturation seems to occur. The behaviour observed for high ablation pulse energy can be attributed to several effects, including the dependence of harmonic amplitude on phase mismatch and scattering or absorption of the driving and harmonic beams by the plasma plume. The solid lines on Fig. 4 correspond to the results of applying a model for HG in these conditions that will be described later (Section IV).

As regards the spatial mapping of the harmonic signals, Fig. 5a illustrates the dependence of harmonic emission as a function of the distance of the driving beam to the target (x coordinate). We observe, in similarity with results of low-order harmonics

generated in ablation plasmas of various materials [23], a fast decay that leads to a vanishing nonlinear response for distances to the target above 3 mm. As shown in Fig. 5a for the early component of the 3rd and 5th harmonics, the decay is faster for the 5th harmonic. As for the previous figure, the solid lines correspond to the application of the frequency conversion model (see Section IV below). We also observe (not shown in the figure) that the late component of the harmonic signal experiences a more pronounced decay than the corresponding early component.

The assessment of the spatial characteristics of the plasma nonlinear response was complemented by *z*-scan measurements. To that purpose, the signal for a given harmonic order was monitored as the position of the driving beam focus moves through the ablation plasma in the laser propagation direction (*z* axis in Fig. 1). Fig. 5b is a representative example for the 5th harmonic measured at x= 0.6 mm. The *z*-scan was performed at two ablation-driving delays (250 ns and 10 μs), which correspond to the maximum frequency up-conversion from fast and slow plume species respectively (early and late components represented by the two maxima of Fig. 3a). For the early component, the amplitude of the harmonic signal decreases symmetrically when the focus of the beam is displaced from the centre towards the boundaries of the plasma. In stark contrast, the *z*-scan for the late component displays a non-symmetrical behaviour as the focus is moved towards each side of the centre of the plasma, and a minimum is found at a position compatible with z= 0. All generated harmonics follow the same *z*-scan trends as described for the 5th harmonic, with the early and late components showing respectively maximum and minimum response near the centre of the plume. Thus, it must be emphasized that the high efficiency conversion found for the 7th harmonic by the second temporal component of the plasma can be enhanced further by

positioning the focal plane of the driving laser a few millimetres in front or behind the centre of the plasma.

3.2. *Optical emission spectra of the ZnS laser ablation plasma.*

In order to provide direct characterization of the dynamic composition of the plasmas we recorded optical emission spectra, both in the absence and in the presence of the driving beam, using different gate widths and delays with respect to the ablation/driving event.

Fig. 6a presents a spectrum of the plasma spontaneous emission, collected with a gate of 100 ns at a delay of 200 ns with respect to the ablation event, in the absence of the driving beam. These acquisition conditions ensure the collection of the early ablation plasma emission. The spectrum is entirely constituted by atomic emission lines mostly assigned to neutral Zn atoms (Zn I) [33], indicating the formation of a mildly ionized plasma upon ablation. The spectrum of this fast plasma atomic component was recorded with acquisition delays up to 1 μs. The spectral line distribution is found practically constant in the short time range, with the global intensity evolving with time in the way shown in the inset of Fig. 6a for the Zn I emission line at 481.05 nm. The most intense Zn atomic emission is observed at around 200 ns, in coincidence with the temporal range at which the harmonic signals present their first maximum (Fig. 3a), followed by a decline to zero above 800 ns. The delayed emission from heavier plasma species was measured using delayed gates and longer acquisition delays. Fig. 6b shows the spectrum collected with a gate delay and width of 1 and 20 μs respectively. In this case there is a very weak indication of the presence of atomic lines and the most salient feature is a broad emission with an apparent maximum centred at around 600 nm. This emission can be attributed to hot plasma nanoparticles [34,35] and after correction by the spectral response of the detection system, a fit of the continuous emission spectrum to Planck's

law yielded a temperature of ca. 2500 K. Some evidence of the presence of nanoparticles in the ablation plasma is provided by atomic force microscopy analysis of the ejected material that has revealed the growth of nanoparticle-assembled films out of the ZnS plasma species deposited on a substrate placed in proximity of the ablation event [28].

Since the driving laser used for these experiments is of nanosecond duration, there is sufficient time for it to change the properties of the plasma plume, in such a way that the effective nonlinear medium results from the combined interaction of the ablation laser with the solid, and the driving laser with the ejected particles. Under this light, we also recorded the plume emission spectra when the driving beam was propagating perpendicularly to the plume expansion direction, at x= 0.6 mm and different delays with respect to the ablating laser, i.e. HG conditions. When ablation and driving lasers temporally overlap (at zero delay), the spectral distribution is identical to that recorded in absence of the driving laser (shown in Fig. 6a). However, as soon as the driving laser is delayed by 100 ns or more with respect to ablation, the spectrum changes markedly, as illustrated in Fig. 7. For short delays (< 1 μs) the overall emission intensity increases with respect to the absence of driving beam, new lines appear that correspond to ionized species (mainly Zn II), and there is hardly any indication of Brehmsstrahlung. However, for delays > 3 μs and during a wide temporal window covering up to ~ 100 μs, a dramatic change is found in the emission spectrum, which is now more than 2 orders of magnitude more intense, includes extensive indication of lines from ionic species and shows pronounced Brehmsstrahlung. Clearly these features are characteristic of a much denser and ionized plasma. For the inset of Fig. 7a we have chosen a neutral (Zn I) and an ionic line (Zn II) and have plotted their intensity as a function of the delay between the ablation event and the driving laser. It must be noted that the temporal structure

found here much resembles the temporal structure found for harmonic emission (see Figure 3), with a rapid component peaking in the few hundreds of nanoseconds and a delayed component most important at 10 μs. It must also be emphasized that the intensity of the later ionic line is almost one order of magnitude higher than that of the early neutral line, thus indicating a considerably larger degree of ionization in the second, delayed plasma component.

4. Calculation of optical-frequency up-conversion in a ZnS ablation plasma

The results reported were obtained with a fundamental beam peak intensity at focus of ca. 4×10^{11} Wcm^{-2}. For such intensity the perturbative approach is adequate in describing the nonlinear interaction of the driving laser, of frequency ω, with a gaseous medium that leads to the generation of odd harmonics of frequencies $n\omega$.[2] The formalism described in [2], which includes phase matching effects in media with inhomogeneous densities, and displacements of the laser focus from the centre of the density distribution, has been applied in order to rationalize the findings of this work.

For a laser ablation plume, the normalized inhomogeneous density distribution of species along the direction of propagation of the driving laser, *z*, at a distance *x* from the target, *S(x, z)*, can be well represented by a Lorentzian function centred in *z*= 0:

$$S(x, z) = \frac{N(x,z)}{N_0(x)} = \frac{1}{1+\left[\frac{2z}{L(x)}\right]^2} \qquad (1)$$

where $N_0(x)$ is the density of nonlinear species at the centre of the plume, and $L(x)$ the full width at half maximum (FWHM) of the gas density distribution at a distance *x* from the target. For a driving Gaussian beam of lowest order of intensity I_ω, the generated harmonics also present lowest-order Gaussian distributions and the intensity of the newly generated coherent light at frequency $n\omega$ is:

$$I_{n\omega} = \alpha(n, \omega, b, k_\omega, k_{n\omega})\left|\chi^{(n)}\right|^2 (I_\omega)^n \, (b\Delta k^{(n)}(x,0))^2 F^{(n)}[b\Delta k^{(n)}(x,z), x, z] \quad (2)$$

In this expression, $\alpha(n, \omega, b, k_\omega, k_{n\omega})$ is a function that includes the dependence with the harmonic order *n*, the confocal parameter of the driving beam *b*, the fundamental frequency ω and the wave vectors of the fundamental and harmonic light beams, k_ω and $k_{n\omega}$ respectively. The n^{th} order susceptibility of the nonlinear medium is denoted by $\chi^{(n)}$, *z* is the distance of the driving beam focus to the centre of the plume and $F^{(n)}[b\Delta k^{(n)}(x,z), x, z]$ is the phase-matching function which depends on *x*, *z* and $b\Delta k^{(n)}(x,z)$. $\Delta k^{(n)}(x,z)$ refers to the wave-vector mismatch between the generated radiation and the driving polarization and has the same spatial dependence as the density of nonlinear species:

$$\Delta k^{(n)}(x,z) = k_{n\omega}(x,z) - nk_\omega(x,z) = S(x,z)\Delta k^{(n)}(x,0) \quad (3),$$

where, in turn, $\Delta k^{(n)}(x,0)$ is proportional to the maximum density $N_0(x)$ of nonlinear scatterers:

$$\Delta k^{(n)}(x,0) = N_0(x)C^{(n)} \quad (4)$$

and $C^{(n)}$ gives the wavelength dependence of the wave-vector mismatch per atom for the n^{th} order HG process.

The phase-matching function is represented by the integral:

$$F^{(n)}\left[b\Delta k^{(n)}(x,z), x, z\right] = \left|\frac{2}{b}\int_{-\infty}^{\infty} \frac{S(x,l)}{(1+i\varepsilon)^{n-1}} exp\left[-i\int_{-\infty}^{l} \Delta k^{(n)}(x,l')dl'\right] dl\right|^2 \quad (5)$$

with $\varepsilon = 2(l-z)/b$.

The integral in (5) was evaluated numerically for odd *n*= 3-9 values in order to analyse the dependence of the intensity of the harmonics generated in the ablation plume of ZnS with the ablation pulse energy, the distance to the target *x* and the position of the focus along the propagation direction of the driving beam, *z* (i.e. the data shown in Figures 4

and 5). This is represented by the corresponding dependences of the function $G^{(n)}$ defined as:

$$G^{(n)}\left[b\Delta k^{(n)}(x,z),x,z\right] = \left(b\Delta k^{(n)}(x,0)\right)^2 F^{(n)}\left[b\Delta k^{(n)}(x,z),x,z\right] \quad (6).$$

In the calculation it was assumed that both the driving and harmonic beams propagate through the plume with negligible absorption.

We examine the evolution of the early component of the harmonic signals with ablation pulse energy E_{ab} by calculating the functions $G^{(3)}$, $G^{(5)}$ and $G^{(7)}$ at the centre of the plume, z= 0, and at a distance x= 0.6 mm from the target surface. According to (4), the dependence of these functions with $b\Delta k^{(n)}(x,0)$ expresses their dependence with $N_0(x)$, the density of species interacting with the driving beam, and consequently with E_{ab} if one assumes a linear dependence between E_{ab} and $N_0(x)$ [36]. For all harmonic orders, a satisfactory comparison of the calculated functions with the experimental curves was found for a value of $L(x)$, the FWHM of the plasma density distribution, of 4 mm for the considered distance to the target. This is shown in Fig. 4, where the calculations appear as solid lines. It is observed that the values of $b\Delta k^{(n)}(x,0)$ for which the harmonic amplitude is maximized at x= 0.6 mm correspond to -6, -10 and -14 for n= 3, 5 and 7 respectively. The values indicate that the medium is negatively dispersive and that phase mismatch increases with harmonic order [2].

For examining the experimental dependence of harmonic signal with the distance to the target x, we calculated the corresponding dependences of $G^{(3)}$, $G^{(5)}$ and $G^{(7)}$. Again in this case the calculation was performed for z= 0, by taking (4) into account and assuming that the density of scatterers in the centre of the plume decays as $N_0(x) = a/x$ with a constant. Considering the optimum values of $b\Delta k^{(n)}(x,0)$ derived in the previous paragraph, we compared the dependence of the measured and calculated harmonic amplitude with x. Fig. 5a illustrates the satisfactory agreement for the early

component of 3rd and 5th harmonics and provides evidence that phase mismatch effects mostly govern this spatial dependence of the harmonic signals.

Finally, to better understand the marked differences in the *z*-scan profile of the early and late component of harmonics (i.e. Fig. 5b) we calculated the dependences of $G^{(3)}$, $G^{(5)}$ and $G^{(7)}$ with z for x= 0.6 mm at different values of $b\Delta k^{(n)}(x,0)$. For the early component (top panel), and as above, the FWHM of the density distribution, $L(x)$, is taken as 4 mm. Fig. 5b displays the good agreement with the experimental behaviour for the value $b\Delta k^{(5)}(x,0) = -10$ that maximizes the harmonic amplitude (see above). For the late component (bottom panel), the experimental behaviour is reasonably reproduced considering values of both $L(x)$ and of $b\Delta k^{(n)}(x,0)$ that are larger than those used for the early component. The curve displayed in the bottom panel of Fig. 5b was calculated for $L(x)$= 14 mm and $b\Delta k^{(5)}(x,0) = -20$. Thus, the dissimilar values of the width of the density distribution and phase mismatch of early and late components, that provide best fits to the data within the approximations of the model, are indicative of the different spatial extension along the driving laser propagation direction and of the dissimilar composition of the species present in the plasma at the explored ablation-driving time delays. These results show that the distribution of late nonlinear precursors along the driving laser propagation direction is considerably wider than that of the early emitters and that at these delays higher populations of bound states and free electrons contribute to create a more dispersive nonlinear medium [7,37].

5. Discussion

As presented herein, the interaction of a 1064 nm, nanosecond driving beam with the IR laser ablation plasma of a ZnS target leads to the generation of low-order odd harmonics that could be detected up to the 9th order with the present experimental setup. The

harmonic signal was found to maximize at two distinct temporal delays with respect to the ablation event, suggesting the presence of two components of the plasma plume moving away from the target at different velocities. The harmonic spectrum is markedly dissimilar for the early and late components; for the former, maximum signals are obtained for the 3^{rd} harmonic and the intensities of higher harmonics drop following a quasi-logarithmic decay, becoming undetectable for the 9^{th} harmonic. The harmonic spectrum observed for late times is anomalous in that it maximizes for the 7^{th} harmonic, is still clearly visible for the 9^{th} harmonic, and lower intensities are emitted at the 5^{th} and 3^{rd} harmonics. As a consequence, the ratio of harmonic intensities of the early to the late component, measured in the centre of the plasma plume, suffers a decrease from the 3^{rd} to the 9^{th} orders across more than two orders of magnitude over the narrow range of harmonics observed. To further accentuate the difference, faster and slower components of the harmonic signals display their own characteristic dependence with plasma coordinates x and z, representing the distance to the target and direction of propagation of the driving beam respectively.

The analyses of plasma emissions by OES help to obtain a consistent picture of the characteristics of the medium at different delays and to clarify the nature of the nonlinear species that are the origin of HG in the plasma plume. The early plasma component is mainly constituted by atomic species, with hardly any evidence of ions. The interaction with the driving laser increases the degree of ionization to a moderate extent. The late component is constituted mainly by nanoparticles, as revealed by their black-body emission. Interaction of the driving laser with this nanoparticle-rich medium causes extensive explosion, fragmentation and ionization, very high particle densities and a high degree of ionization, with abundant free electrons. The direct measurement of the temporal delay where harmonic emission maximizes as a function of the distance

from the target allows an estimation of the central speed of both components. The early component propagates at > 3000 m/s, a high velocity value characteristic of atomic species in nanosecond ablation plumes [18,19]. Among the possible neutral atom emitters, it is expected that Zn plays a significantly more important role than S due to its larger polarizability [38].

To provide further support to the assumption that neutral Zn atoms constitute the main nonlinear component of the 1064 nm, ZnS ablation plasma in the early temporal region, we characterized the behaviour of the harmonics generated in an ablation plume of a metallic Zn target. Using identical conditions as those employed for ZnS, we observed harmonic generation with intensity of the order of that in ZnS and maximizing in the same temporal region (200-300 ns). Moreover, we compared the intensity of the spontaneous emission line from neutral Zn atoms at 334 nm ($4s4d\,^3D - 4s4p\,^3P$) (see Fig. 6a) with that of the 3rd harmonic. The ratio measured for a Zn target ($4x10^{-3}$ approx.) is compatible with that found for ZnS. We believe that the three pieces of evidence acquired from the comparison of the ablation of Zn and ZnS targets (similar 3rd harmonic intensity for the early component, same temporal maximum and same ratio with respect to spontaneous atomic Zn emissions) sustain the conclusion that early nonlinear emitters in the ZnS ablation plasma are indeed Zn atomic species.

As mentioned, clusters and nanoparticles are described to be formed in nanosecond laser ablation plumes of various materials by recombination of atomic and molecular species near the target surface at some delays with respect to the ablation event [15,16, 18-20]. In our case, the temporally delayed component of the plasma is shown by OES to be mainly constituted by nanoparticles and the results obtained provide enough evidence of extensive atomization and ionization of these nanoparticles by the driving laser. At the long time delays measured for the slow component, the driving laser

generates a fragmented and ionized secondary plasma, where the resulting excited atoms and ions act as delayed nonlinear species and yield a particularly high conversion efficiency towards higher harmonic orders. Previous studies have revealed the alteration of nanoparticle population in laser ablation plasmas by a delayed probe laser pulse, leading to an increased atomic population [39-42]. We believe that the Zn II species may be the main contributor to HG in this component. Ions are known to present lower HG efficiency due to their lower polarizability, but it is also known that they tend to generate harmonics at higher orders than neutrals, at least in the strong field regime. Kulander et al. [43] showed that the ratio of harmonic emission from neutrals to ions was > 1 for low harmonic orders but < 1 for higher harmonic orders. This expected trend coincides with the ratios of the early vs. late harmonic emission component in this experiment, and thus constitutes an additional element for the assignment of the first component to neutral species and the late component to ionic species. In fact, the particularly favoured 7^{th} order nonlinear response at long delays is feasibly related with the enhancement of the nonlinear susceptibility via a seven-photon resonant $3d^{10}4s$ – $3d^{9}4s^{2}$ transition of singly charged Zn ions at 65441.41 cm^{-1} [33]. This transition could also play a role in the significant emission of the 9^{th} harmonic that could be enhanced via an intermediate seven-photon resonant state.

The above considerations serve to explain the origin of the two temporal components of the harmonic signal and the harmonic spectrum of each component. Crucially, the characteristics of the secondary plasma created by the driving beam play a defining role on the effective nonlinear medium and provide a route for the control of harmonic emission, mediated by the laser modification of the density and degree of ionization of this plasma. Elementary calculations of the phase matching integrals indicate that phase matching effects dominate the dependence of harmonic signals with the ablation laser

pulse energy and with the position of the driving beam focus across the spatial dimensions of the plume. This comparison also serves to estimate the different widths of the density distribution of the fast Zn neutral atoms and of the slow singly charged Zn ions that are originated by fragmentation of nanoparticles (around 4 and 14 mm respectively at a 0.6 mm above the target). Earlier investigations have demonstrated that atomic species in nanosecond ablation plumes display distinct angular distributions [44,45] with a stronger forward bias in the direction normal to the target surface with increasing charge state of the atom. The results obtained herein display a tendency opposed to this general trend. However, one should keep in mind that the Zn ions, considered to be the main origin of the harmonic signals at longer times, are the constituents of a secondary plasma created by interaction of the driving beam with a slow nanoparticle population and therefore their angular distribution reflects that of their precursor population.

6. Conclusions

We demonstrate odd harmonic generation up to the 9^{th} order of a 1064 nm fundamental driving beam propagating through a nanosecond infrared laser ablation plasma plume of a ZnS target. The harmonic signals present two temporal components that are ascribed to fast neutral Zn atoms and to singly charged Zn ions, the latter resulting from fragmentation by the driving laser of slower ZnS nanoparticles. For Zn ions, the enhancement of the nonlinear susceptibility by a seven-photon resonance accounts for the favoured nonlinear response of the late 7^{th} order signal. Calculations of the phase matching integrals reveal the influence of phase matching in the behaviour of harmonic signals with ablation pulse energy and spatial coordinates of the plasma plume. These calculations allow an estimation of the width of the distribution of Zn neutrals and

nanoparticles, at about 0.6 mm above the target, of around 4 and 14 mm respectively. Thus, it is concluded that optical harmonic generation in the infrared laser ablation plasma of ZnS serves to assess the presence of atomic and nanoparticles and their differing spatial and temporal distributions. The driving beam creates a secondary plasma and the possibility of modifying its density and degree of ionization opens new routes for finding efficient media for generation of coherent vacuum ultraviolet light by nonlinear frequency up-conversion.

Acknowledgements

Funding has been provided by Ministerio de Economía y Competitividad (MINECO) of Spain under Project CTQ2013-43086-P. I.L-Q., A.B-C. and M.O. thank respectively MINECO, for a FPI fellowship (BES-2011-044738), CSIC, for a JAE-TEC 2010 contract and CSIC for a contract. Fruitful discussions with Dr. Mikel Sanz and Prof. A. Gonzalez-Arroyo are acknowledged.

References

[1] J. F. Reintjes, Optical Parametric Processes in Liquids and Gases, 1984, New York, Academic Press.

[2] A. Lago, G. Hilber and R. Wallenstein, Phys. Rev. A, 1987, **36**, 3827.

[3] C. J. Joachain, N. J. Kylstra, and R. M. Potvliege., Atoms in Intense Laser Fields, 2011, Cambridge University Press.

[4] P. B. Corkum, Phys. Rev. Lett., **71**, 1994 (1993).

[5] P. Jaeglé, Coherent Sources of XUV Radiation: Soft X-Ray Lasers and High-Order Harmonic Generation, 2006, New York, Springer

[6] P. Lee, D. V. Giovanielli, R. P. Godwin and G. H. McCall, App. Phys. Lett., **24**, 406 (1974).

[7] W. Theobald, C. Wülker, F. P. Schäfer and B. N. Chichkov, Opt. Commun., **120**, 177 (1995).

[8] R. Ganeev, Plasma Harmonics, 2014, Boca Raton, CRC Press.

[9] S.-Y. Zhao, P.-L. Zhang, G.-Z. Zhang and W.-Z. Zhao, Appl. Opt., **28**, 4521(1989).

[10] R. A. Ganeev, C. Hutchison, I. Lopez-Quintas, F. McGrath, D. Y. Lei, M. Castillejo and J. P. Marangos, Phys. Rev. A, **88**, 033803 (2013).

[11] R. A. Ganeev, T. Witting, C. Hutchison, V. V. Strelkov, F. Frank, M. Castillejo, I. Lopez-Quintas, Z. Abdelrahman, J. W. G. Tisch and J. P. Marangos, Phys. Rev. A, **88**, 033838 (2013).

[12] T. Ozaki, L. B. Elouga Bom, J. Abdul-Hadi and R. A. Ganeev, Laser and Particle Beams, 2010, **28**, 69.

[13] H. Singhal, P. A. Naik, M. Kumar, J. A. Chakera and P. D. Gupta, J. App. Phys., **115**, 033104 (2014).

[14] R. A. Ganeev, M. Suzuki, S. Yoneya and H. Kuroda, J. Phys. B, **48**, 165401 (2015).

[15] M. Jadraque, A. B. Evtushenko, D. Ávila-Brande, M. López-Arias, V. Loriot, Y. G. Shukhov, L. S. Kibis, A. V. Bulgakov and M. Martín, J. Phys. Chem C, **117**, 5416 (2013).

[16] D. Yadav, V. Gupta and R. K. Thareja, J. App. Phys., **106**, 064903 (2009).

[17] A. A. Puretzky, D. B. Geohegan, G. B. Hurst, M. V. Buchanan and B. S. Luk'yanchuk, Phys. Rev. Lett., **83**, 444 (1999).

[18] O. Albert, S. Roger, Y. Glinec, J. C. Loulergue, J. Etchepare, C. Boulmer-Leborgne, J. Perrière and E. Millon, App. Phys. A, **76**, 319 (2003).

[19] F. Claeyssens, M. N. R. Ashfold, E. Sofoulakis, C. G. Ristoscu, D. Anglos and C. Fotakis, J. App. Phys., **91**, 6162 (2002).

[20] A. Mohanta and R. K. Thareja, J. App. Phys., 106, 124909 (2009).

[21] M. Oujja, R. de Nalda, M. López-Arias, R. Torres, J. P. Marangos and M. Castillejo, Phys. Rev. A, **81**, 043841 (2010).

[22] R. de Nalda, M. Lopez-Arias, M. Sanz, M. Oujja and M. Castillejo, Phys. Chem. Chem. Phys., **13**, 10755 (2011).

[23] M. López-Arias, M. Oujja, M. Sanz, R. de Nalda, R. A. Ganeev and M. Castillejo, Mol. Phys., **110**, 1651 (2012).

[24] M. López-Arias, M. Oujja, M. Sanz, R. A. Ganeev, G. S. Boltaev, N. K. Satlikov, R. I. Tugushev, T. Usmanov and M. Castillejo, J. App. Phys., **111**, 043111 (2012).

[25] I. Lopez-Quintas, M. Oujja, M. Sanz, M. Martín, R. A. Ganeev and M. Castillejo, App. Surf. Sci., **278**, 33 (2013).

[26] M. Oujja, A. Benítez-Cañete, M. Sanz, I. Lopez-Quintas, M. Martín, R. de Nalda and M. Castillejo, App. Surf. Sci., **336**, 53 (2015).

[27] Wide Bandgap Semiconductors: Fundamental Properties and Modern Photonic and Electronic Devices, K. Takahashi, A. Yoshikawa, A. Sandhu (Eds.), 2007, Berlin, Springer-Verlag.

[28] M. Sanz, M. López-Arias, E. Rebollar, R. Nalda and M. Castillejo, J. Nanopart. Res., **13**, 6621 (2011).

[29] M. Sanz, M. López-Arias, J. F. Marco, R. de Nalda, S. Amoruso, G. Ausanio, S. Lettieri, R. Bruzzese, X. Wang and M. Castillejo, J. Phys. Chem. C, **115**, 3203 (2011).

[30] I. Lopez-Quintas, V. Loriot, D. Avila, J. G. Izquierdo, E. Rebollar, L. Banares, M. Castillejo, R. de Nalda and M. Martin, Phys. Chem. Chem. Phys., **18**, 3522 (2016).

[31] J. Álvarez-Ruiz, M. López-Arias, R. Nalda, M. Martín, A. Arregui and L. Bañares, App. Phys. A, **95**, 681 (2008).

[32] M. Oujja, A. Benítez-Cañete, I. López-Quintás, M. Martín, R. de Nalda and M. Castillejo, J. Phys.: Conference Series, **635**, 122002 (2015).

[33] http://physics.nist.gov/PhysRefData/ASD/lines_form.html

[34] S. Amoruso, G. Ausanio, R. Bruzzese, M. Vitiello and X. Wang, Phys. Rev. B, **71**, 033406 (2005).

[35] S. S. Harilal, N. Farid, A. Hassanein and V. M. Kozhevin, J. App. Phys., **114**, 203302 (2013).

[36] D. W. Bäuerle, Laser Processing and Chemistry, 2011, Berlin, Springer-Verlag.

[37] A. B. Fedotov, N. I. Koroteev and A. M. Zheltikov, Laser Physics, **5**, 812 (1995).

[38] http://cccbdb.nist.gov/polcalc1.asp

[39] S. Noël and J. Hermann, App. Phys. Lett., **94**, 053120 (2009).

[40] J. Uebbing, J. Brust, W. Sdorra, F. Leis and K. Niemax, Appl. Spectrosc., **45**, 1419 (1991).

[41] S. Amoruso, R. Bruzzese, X. Wang, G. Ausanio and L. Lanotte, J. Phys. B, **40**, 1253 (2007).

[42] J. González, C. Liu, J. Yoo, X. Mao and R. E. Russo, Spectrochim. Acta B, **60**, 27 (2005).

[43] J. L. Krause, K. J. Schafer and K. C. Kulander, Phys. Rev. Lett., **68**, 3535 (1992).

[44] T.-J. Andrea and R. Klaus, J. Phys. D, **32**, 2827 (1999).

[45] Y. Nakata, J. Muramoto, T. Okada and M. Maeda, J. App. Phys., **91**, 1640 (2002).

Figure captions

FIG. 1 Scheme of the experimental set up used for measuring low-order (3^{rd}-9^{th}) HG of a fundamental IR driving laser in a plasma induced by laser ablation at 1064 nm. The inset shows the interaction region in detail.

FIG. 2 Log-log plot of the 5^{th} harmonic signal as a function of the energy of the laser driving pulse focussed at z= 0, in the 1064 nm ablation plume of ZnS measured at x= 0.6 mm from the surface of the target; a) and b) refer to measurements at an ablation-driving laser delay of 250 ns and 10 μs respectively. The ablation pulse energy is 20 mJ. The slopes of the linear fits are compatible with a fifth order nonlinear process.

FIG. 3 Temporal behaviour of harmonics in the 1064 nm ablation plume of ZnS: a) Normalized signals of the 3^{rd} to the 9^{th} harmonic orders of the IR driving laser, focused at z= 0, in a ZnS ablation plasma, as a function of the delay between the ablation event and the arrival of the driving laser, measured at x= 0.6 mm from the surface of the target. Intensities and delays are represented in logarithmic scales for better visualization. b) Optimum delay for maximum value of the early component of the harmonic signal as a function of the distance of the driving beam to the target along x. The continuous straight line corresponds to an average velocity of expansion of nonlinear species of 3400 m/s. For these measurements the ablation pulse energy is 20 mJ and the laser driving peak intensity is $4x10^{11}$ Wcm^{-2}.

FIG. 4 Experimental dependence of the normalized early component (peaked at an ablation-driving delay of around 250 ns) of the 3^{rd}, 5^{th} and 7^{th} harmonics (squares, circles, and triangles respectively) with ablation pulse energy. The driving laser propagates at x= 0.6 mm from the target and is focused at the centre of the ablation

plume (z= 0). The continuous lines represent the dependence of harmonic intensity calculated as a function of $b\Delta k^{(n)}(x,0)$ (see text). The laser driving peak intensity is $4x10^{11}$ Wcm^{-2}.

FIG. 5 Spatial behaviour of harmonic emission. a) Harmonic intensity (normalized to the value at x= 0.6 mm) as a function of the distance of the driving beam to the target for z= 0. For each measurement the ablation-driving laser delay was set at the value for optimum harmonic signal. Full red squares and blue circles refer to the experimental early 3^{rd} and 5^{th} harmonic signals. The continuous red and blue lines are the result of the calculation for the respective harmonics (see text). b) z-Scans of the 5^{th} harmonic signal as a function of the position of the driving beam focus with respect to the centre of the ablation plasma (z= 0) in the propagation direction (shown by a black arrow) for x= 0.6 mm. The ablation-driving delays are set at 250 ns (and 10 μs), for measuring the early (top panel) and late (bottom panel) temporal components of the harmonic signal. The continuous lines represent the calculation for $L(x)$= 4 mm, $b\Delta k^{(n)}(x,0) = -10$ (top) and $L(x)$= 14 mm, $b\Delta k^{(n)}(x,0) = -20$ (bottom) (see text). The laser driving peak intensity is $4x10^{11}$ Wcm^{-2}.

FIG. 6 Optical spontaneous emissions from a ZnS plume generated by ablation at 1064 nm with pulses of 20 mJ in the absence of driving beam: a) Spectrum collected with a 100-ns wide acquisition gate delayed 200 ns with respect to ablation; the emissions are mainly assigned to neutral Zn and weak evidence for S atomic lines, and a minor contribution from an ion Zn II line (see text). The inset shows the evolution of the Zn I emission at 481.05 nm with acquisition delay. b) Spectrum of spontaneous emission obtained with a 20-μs acquisition gate delayed 1 μs with respect to ablation. In this

temporal window the emissions are dominated by black body radiation from nanoparticles, with minor contributions from atomic lines (see text).

FIG. 7 Optical emission spectra from a ZnS plume generated by ablation at 1064 nm with pulses of 20 mJ in the presence of the driving beam: a) Spectrum detected for 400 ns ablation-driving delay. Emission lines are assigned to neutral Zn I, ionic Zn II, and second orders of shorter wavelength Zn lines. The inset shows the intensity of the strongest Zn I line (at 481.05 nm) and the strongest Zn II line (at 491.16 nm) as a function of ablation-driving delay. b) Spectrum detected for 12 μs ablation-driving delay. The plasma shows a high degree of ionization, with most lines corresponding to ionic Zn II, and strong Brehmsstrahlung. Scales in a) and b) are in arbitrary units but are comparable. The laser driving peak intensity for these measurements is $4x10^{11}$ Wcm^{-2}.

Figure 1 (colour online)

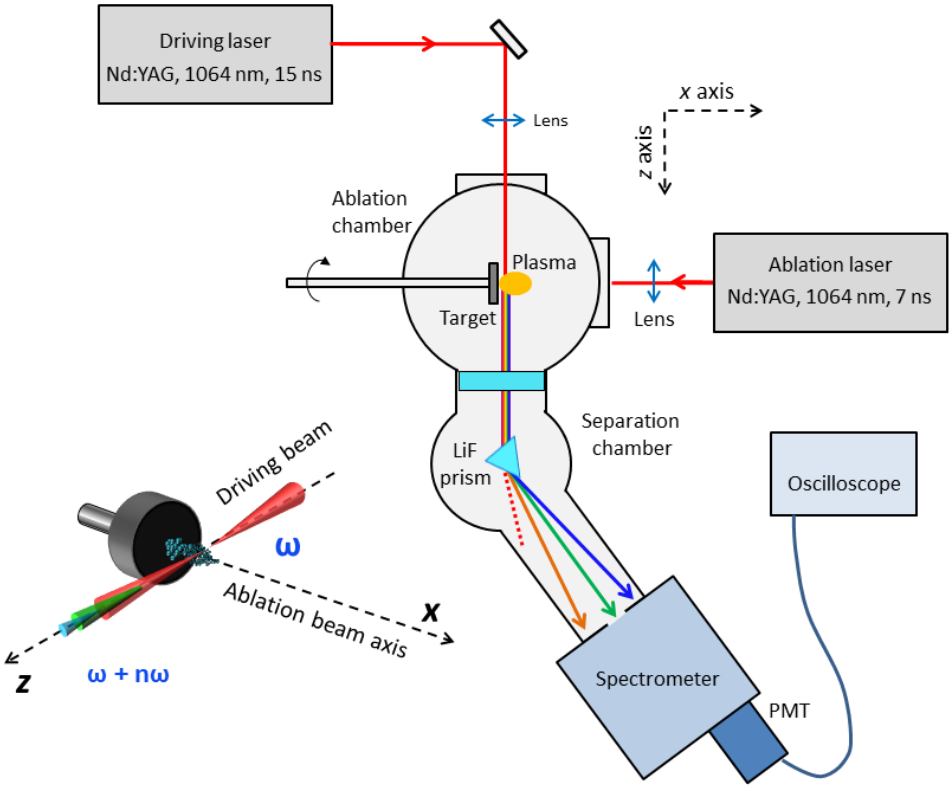

Figure 2 (colour online)

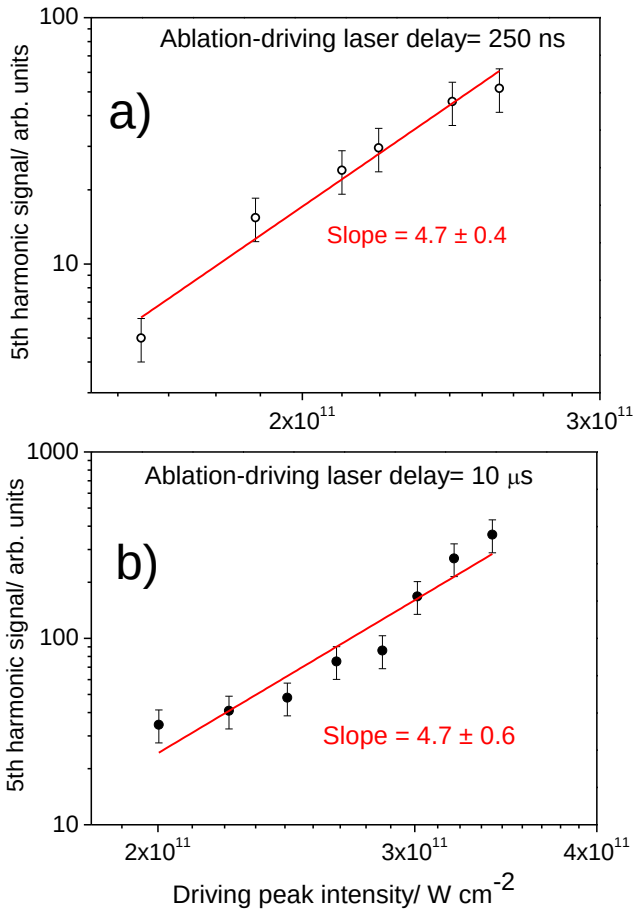

Figure 3 (colour online)

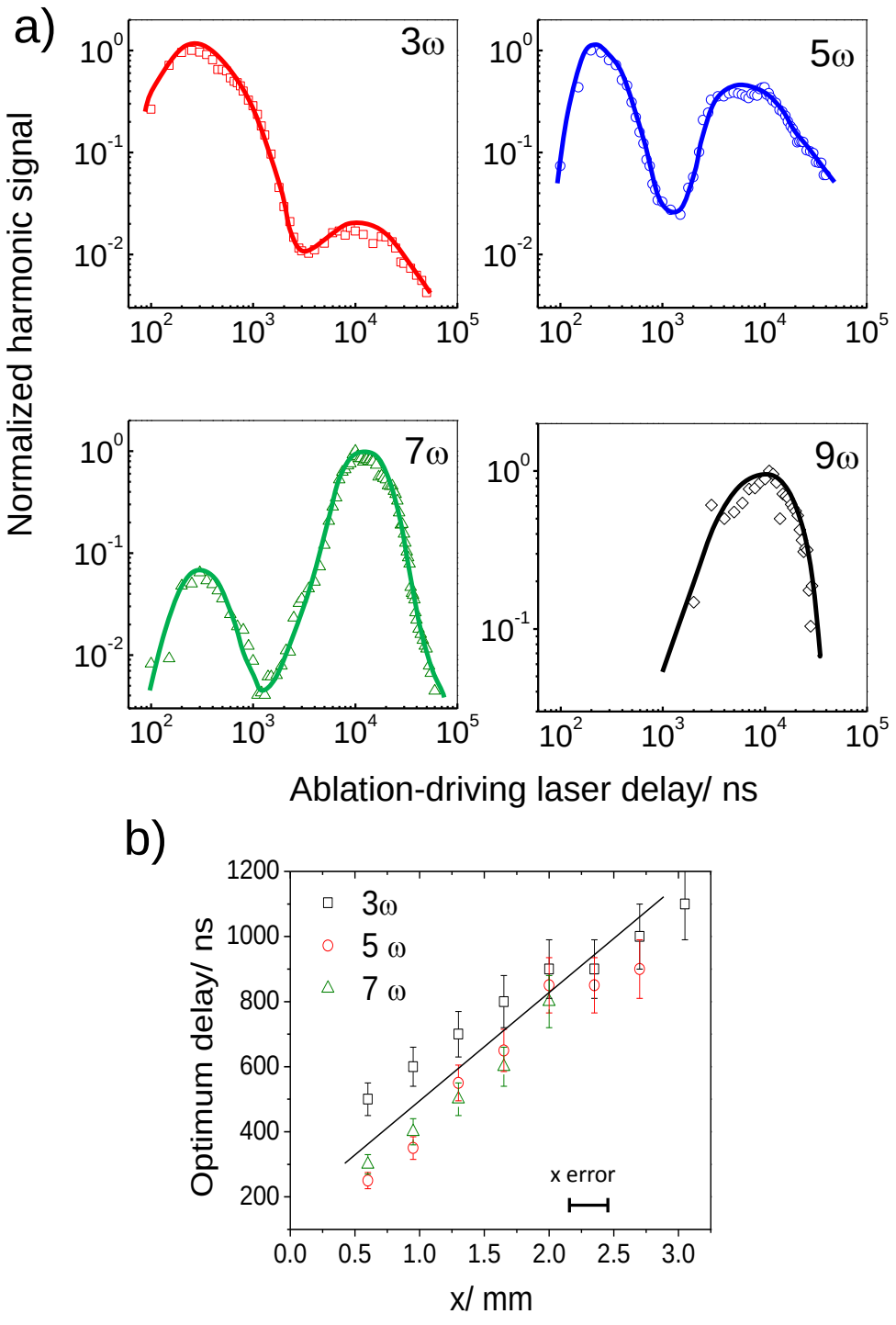

Figure 4 (colour online)

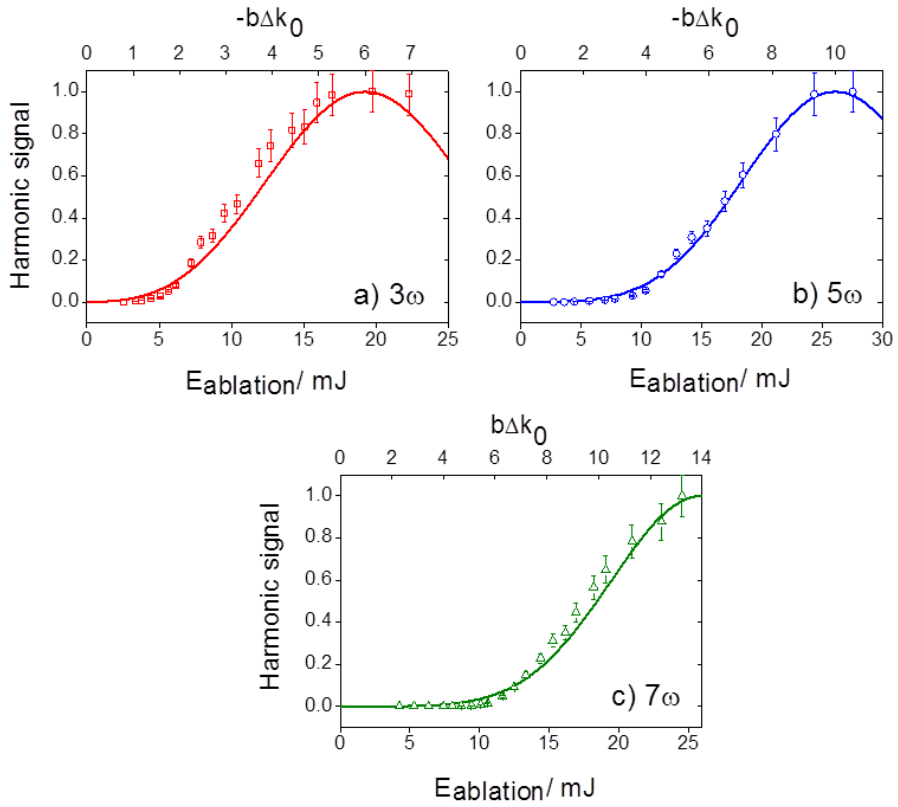

Figure 5 (colour online)

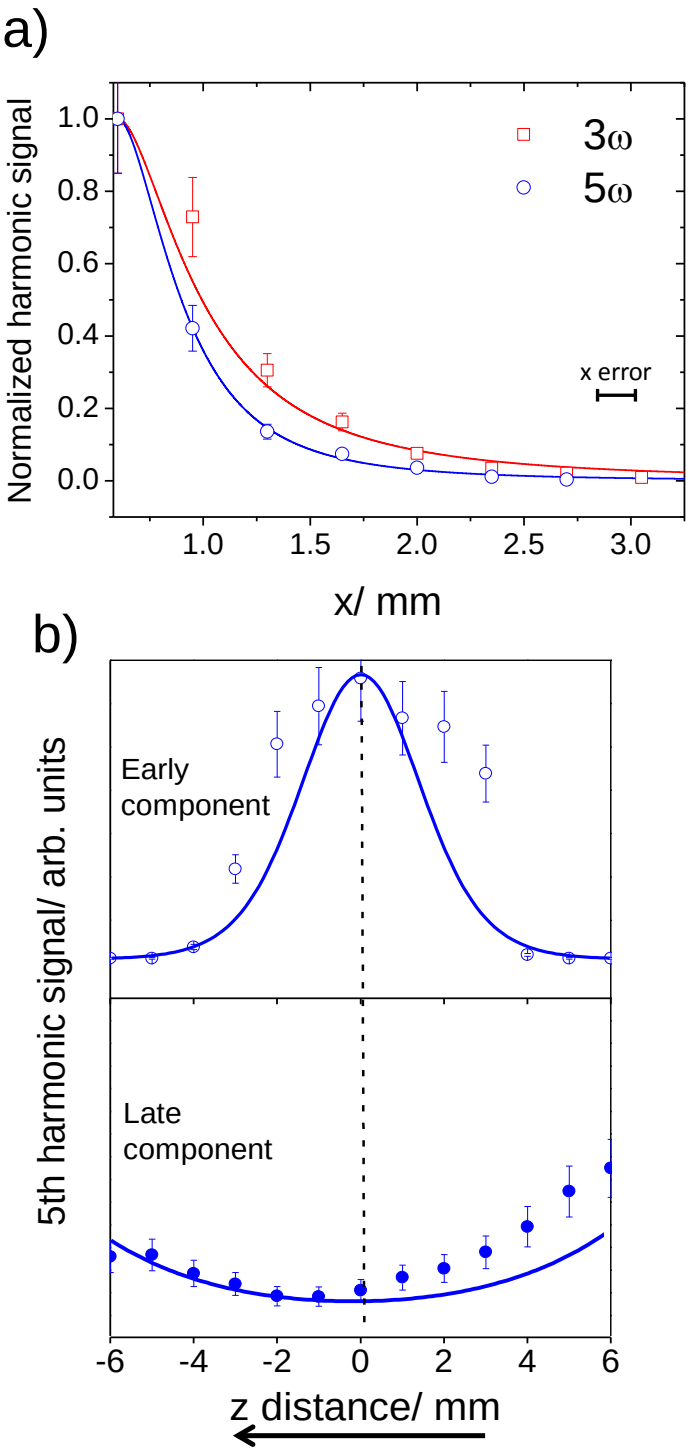

Figure 6 (colour online)

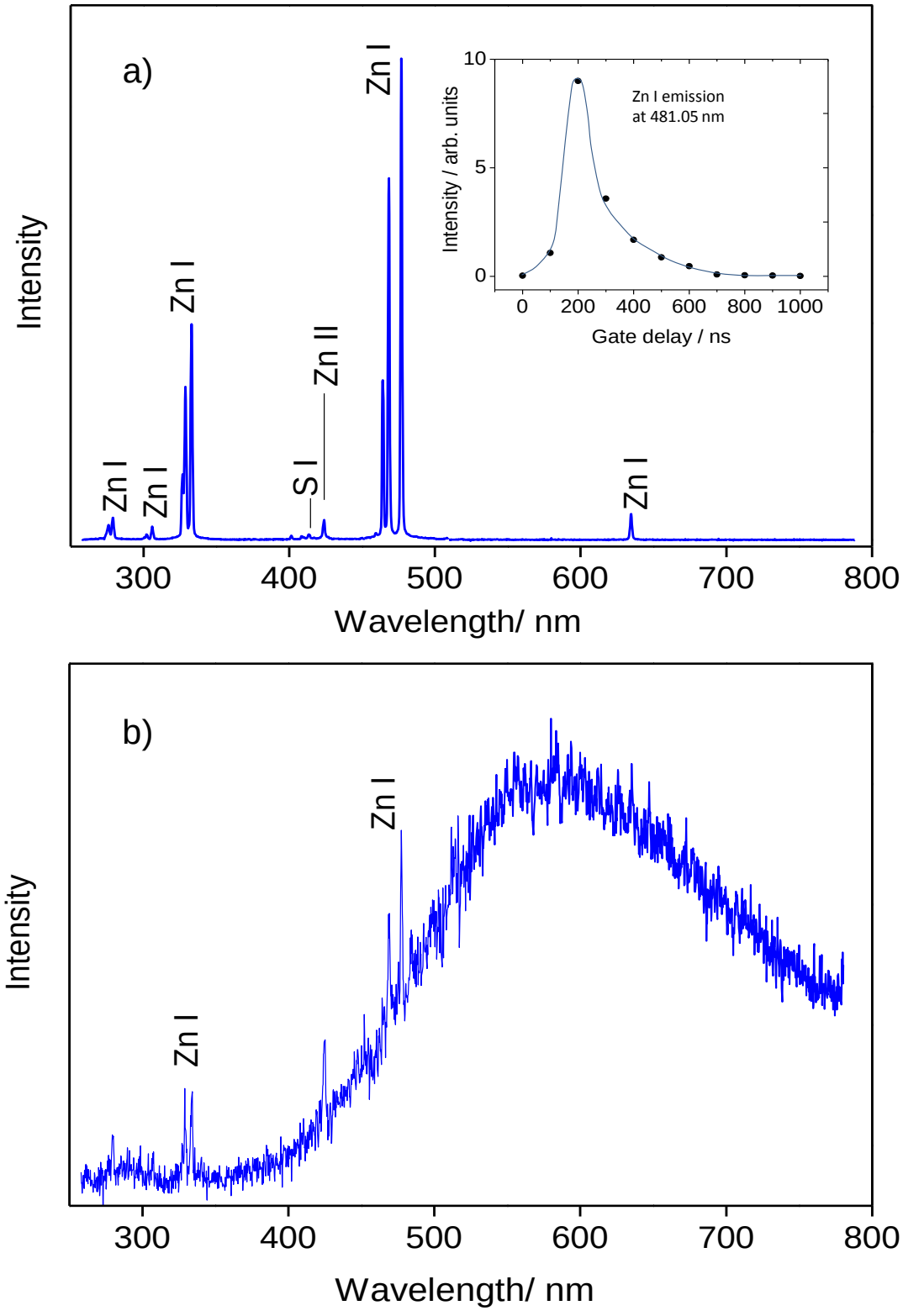

Figure 7 (colour online)